archaeometry

Archaeometry **56**, 2 (2014) 331–350 doi: 10.1111/arcm.12018

RESISTIVITY TOMOGRAPHY IMAGING OF THE SUBSTRATUM OF THE BEDESTAN MONUMENTAL COMPLEX AT NICOSIA, CYPRUS*

M. COZZOLINO and P. MAURIELLO

Department of Science and Technology for Environment and Territory, University of Molise, Campobasso, Italy

and D. PATELLA†

Department of Physics, University Federico II, Naples, Italy

In the framework of the EU–UNDP project 'Rehabilitation of Old Nicosia' (Cyprus, 2004–9), a high-resolution geoelectrical survey has been performed inside the partially ruined monumental complex of St Nicholas of the English, now called the Bedestan, which was designed to become a venue space for cultural activities. The aim was to detect buried traces of a Byzantine basilica of the sixth century, on the ruins of which, according to tradition, the construction of St Nicholas was begun in the 12th century. The survey has been conducted on the floor of the monument, using a dipole–dipole electrode array along two perpendicular sets of profiles. In order to model the resistivity distribution, the probability-based electrical resistivity tomography inversion (PERTI) method has been applied. Sets of aligned blocks with resistivity in the range 100–400 ohm·m, bounding a three-room rectangular space, and traces of a rounded structure with mean resistivity about 150 ohm·m, appearing at one extremity of the central room, are the main resistive features recognized down to 4 m depth, within a conductive background with resistivity in the range 20–40 ohm·m. Altogether, these resistive features, showing in plan the shape of a church characterized by a central nave with an apse and two side aisles, have been interpreted as an evidence of the existence of remains of the earlier Byzantine basilica. Moreover, small volumes with resistivity in the range 10–12.6 ohm·m have been found, scattered underneath the whole surveyed area. Taking into account the PERTI results, ground-truth has been performed in two sites, designed to become two permanent protected exposures of the archaeological findings beneath the floor of the newly restored Bedestan. At one site, excavations detected remains of masonry in correspondence of the alignment of resistive blocks at the left margin of the left side aisle of the churchlike structure. At the other site, graves, entirely filled with wet debris in an alluvial soil matrix, have, instead, been found in correspondence with the greatest conductive volume, detected outside the perimeter of the churchlike structure. Both findings have been dated back to the sixth century. Since the Bedestan case-history is one of the first applications of the PERTI algorithm to real field data sets, its performance has been tested using the well-known ERTLab™ commercial software as benchmark. The comparison has shown a general consistency between the two inversions, and also confirmed the much higher computing speed, better filtering capacity and greater versatility of the PERTI algorithm, already outlined in a previous paper where only synthetic models were tested.

KEYWORDS: NICOSIA, CYPRUS, BEDESTAN MONUMENT, FOUNDATIONS, ELECTRICAL RESISTIVITY TOMOGRAPHY, BYZANTINE BASILICA RELICS, SIXTH CENTURY

*Received 26 February 2012; accepted 21 June 2012
†Corresponding author: email patella@na.infn.it

INTRODUCTION

The monumental complex of the Bedestan (Fig. 1) is located on the Turkish side of the walled city of Nicosia, Cyprus, a few metres south of the Selimiye mosque. Building work started in the 12th century, to host the Catholic church of St Nicholas of the English. It was later enlarged with some Gothic annexes by the Lusignan dynasty (1192–1489). After some further changes in the Venetian period (1489–1570), the building was donated to the Greek Orthodox Metropolis. In the Ottoman period (1570–1878), the complex was called the Bedestan, meaning 'covered market', and used mostly for the trade of grain and textile products (Jeffery 1918; Boase 1977). Historical sources report that the Bedestan was built on the ruins of a sixth-century Byzantine basilica (Qantara 2008), but the shape, size and location of the earlier church have always remained uncertain. The building with its different architectural styles is visibly of hybrid nature. Collapses and episodes of destruction, occurring during the past centuries, were only partially restored, so that up to as recently as 2004 the appearance of the monument was one of a partially ruined historical edifice.

A plan of consolidation and conservative restoration of the Bedestan complex was approved in late 2004 within the EU-funded 'Rehabilitation of Old Nicosia' project, implemented by the UN 'Partnership for the Future' development programme. A strong motivation for the intervention was the dual nature of the Bedestan, situated as it was halfway between an archaeological ruin and a disused building. It was felt, therefore, that the dedication of the monument to cultural activities would give a lofty sense of meaning to the fragmentary elements that had survived destruction (www.undp-pff.org/1).

The prior phase of the project consisted of the analysis and evaluation of the modifications undergone by the building in the course of time. A stratigraphic analysis of the exposed walls of the complex allowed the various construction phases from the 10th century onwards to be geometrically delineated (Cessari and Gigliarelli 2007). However, no clear physical evidence emerged from this analysis as to the presence of the earlier Byzantine basilica. For this reason, we were asked to plan a geoelectrical resistivity tomography (ERT) survey in order to identify traces of the presence of the earlier basilica beneath the floor of the Bedestan complex.

Geoelectrics is one of the most reliable prospecting tools in the field of cultural heritage, thanks to the technological and methodological developments of recent years, which have made it a fast, target-oriented method. The resistivity parameter, on which the method is based, has so large a variability as to allow the great majority of buried structures and bodies of archaeological and architectural interest to be distinguished from the hosting material. To enhance the resolution power of the method, great help is provided by the ERT approach, which implies handling of large data sets. ERT is very popular in the field of cultural heritage, and a wealth of successful indoor and outdoor applications are found in the current specialized literature (e.g., Noel and Xu 1991; Cammarano *et al*. 1997; Tsokas and Tsourlos 1997; Mauriello *et al*. 1998; Candansayar *et al*. 1999; Kampke 1999; Matias *et al*. 2006; Ranieri *et al*. 2007; Cardarelli *et al*. 2008; Drahor *et al*. 2008a,b; Gaffney 2008; Papadopoulos *et al*. 2008; Abu Zeid *et al*. 2009; Bavusi *et al*. 2009; Hecht 2009; Nuzzo *et al*. 2009; Tsokas *et al*. 2009; Mol and Preston 2010).

A preliminary resistivity map of the Bedestan substratum deduced from our data set was already included in the report by Cessari and Gigliarelli (2007). That map was used simply to show the ERT potential in solving the question raised. Therefore, the aim of this paper is to present in detail all the quantitative aspects related to the Bedestan ERT survey. In the following sections, we provide at first an outline of the ERT acquisition plan, then we give a thorough description of the ERT inversion results, obtained using the new PERTI (Probability-based ERT

Figure 1 *The Bedestan complex, previously St Nicholas Church of the English, at Nicosia, Cyprus, before restoration: (a) an aerial view of the whole complex and (b) a frontward view of St Nicholas nave (from www.undp-pff.org/2).*

Inversion) method (Mauriello and Patella 2009), and finally we suggest an interpretation of the 3D resistivity model of the Bedestan substratum in terms of archaeological and architectural features.

This contribution provides one of the first applications of the PERTI method to large field data sets, which were not considered in the presentation of the algorithm by Mauriello and Patella (2009), where only examples drawn from synthetic modelling were discussed. Thus, a comparison is also included between the PERTI results and those obtained using the renowned ERTLab™ inversion software (www.mpt3d.com, www.geoastier.com), in order to highlight the main features of the new method.

OUTLINE OF THE ERT FIELD TECHNIQUE

In indoor ERT applications to archaeology, a suitable measuring modality is the dipole–dipole source–receiver coupling, because of its greater compactness and sensitivity to both the lateral location and the depth evaluation of anomalous source bodies (Ward 1990).

Figure 2 shows the ERT procedure along a profile, where, for simplicity, only one pair of dipoles at a generic placement is sketched. In practice, the modern equipment comprises a fully automated multichannel resistivity meter with multi-electrode switching capability, with an integrated PC for full control of the acquisition process and storage of data.

For a preliminary evaluation of the ERT information content from a grid of nodal points as in Figure 2, apparent resistivity contour lines are mapped at constant linear or logarithmic intervals. A high-resolution 2D extension of the ERT technique consists of combining multiple sets of profiles in order to investigate a whole area instead of a single line. The consequent 3D distribution of the apparent resistivity at the datum points can be imaged by drawing sequences of pseudosections or pseudomaps at increasing pseudodepths.

It must be remarked that any of the apparent resistivity representations, as described above, has only a rough relationship with the real resistivity pattern, whose modelling is the ultimate purpose of the survey. In fact, the shape and amplitude of the anomalies, which strictly represent shifts

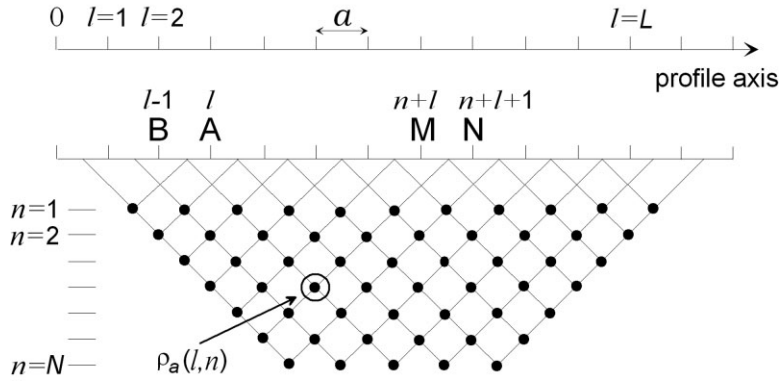

Figure 2 *The ERT technique with a dipole–dipole array. 'A' and 'B' are the electrodes of the active dipole, used to inject current into the subsoil, 'M' and 'N' are the electrodes of the passive dipole, used to measure the potential drop. The index l = 1, . . . , L defines the placement of the active dipole along the profile, while n = 1, . . . , N indicates the number of steps separating the active from the passive dipole, as well as the point of attribution of the apparent resistivity, $\rho_a(l,n)$. The last level n = N is only indicative. The deepest reachable level depends on the length of the profile and consists of a unique attribution point located at the bottom vertex of the triangle-shaped grid.*

among different apparent resistivity values, depend not only on the unknown true resistivity pattern and data density, but also on contamination due to even small inhomogeneities close to electrodes. In order to remove corrupting effects and model the survey targets as accurately as possible, a numerical inversion is needed to convert apparent into real resistivity images.

THE ERT SURVEY AT THE BEDESTAN

The ERT survey inside the Bedestan area was performed using a dipole–dipole array. Two perpendicular sets of profiles were arranged as in Figure 3. Table 1 lists all of the acquisition parameters for each ERT profile, numbered as in Figure 3. A data set of about 17 000 datum points was collected.

The MAE A3000^{TM} resistivity meter (www.mae-srl.it) was used. This instrument integrates all of the elements to carry out fast multi-electrode prospecting from a basic 32-electrode device, up to a maximum of 256 electrodes, using external commutating boxes. The 60 W internal power supply can be increased up to 250 W. The unit is fully computerized and all the operative functions are selected using a menu on a LCD monitor with an integrated touch screen. The solution adopted to place the electrodes on the floor inside the Bedestan complex consisted of steel nails of length 0.1 m hammered into the interstices between bricks, as shown in Figure 4.

As is known, a disadvantage of the dipole–dipole array is the fast decrease of the signal strength and, consequently, of the signal-to-noise ratio for increasing values of n (Ward 1990). There are three ways to overcome this problem (Loke 2012). The first one is to increase the intensity of the injected current. The MAE transmitter unit may provide a maximum current of 5 A, by setting the output voltage to the minimum value of 50 V and the internal power to the maximum value of 250 W. The second way is to make recourse to the stacking process of the

Figure 3 *The ERT survey planning inside the Bedestan monument. Full and dashed lines over the sketched topographic map of the complex indicate longitudinal and transversal ERT profile sets, respectively. Table 1 reports the acquisition parameters of each ERT profile.*

Table 1 *A list of the acquisition parameters of all of the ERT profiles drawn in Figure 3*

Longitudinal profiles					*Transversal profiles*				
No.	*Length (m)*	*Step (m)*	n_{max}	*Datum points*	*No.*	*Length (m)*	*Step (m)*	n_{max}	*Datum points*
1	13.5	0.5	25	325	33	13.5	0.5	25	325
2	14.5	0.5	27	378	34	13.5	0.5	25	325
3	16.5	0.5	29	435	35	13.5	0.5	25	325
4	16.5	0.5	29	435	36	13.5	0.5	25	325
5	16.5	0.5	29	435	37	12	0.5	22	253
6	16.5	0.5	29	435	38	12	0.5	22	253
7	16.5	0.5	29	435	39	12	0.5	22	253
8	16.5	0.5	29	435	40	12	0.5	22	253
9	14.5	0.5	27	378	41	12	0.5	22	253
10	14.5	0.5	27	378	42	12	0.5	22	253
11	14.5	0.5	27	378	43	11.5	0.5	21	231
12	14.5	0.5	27	378	44	11.5	0.5	21	231
13	16.5	0.5	29	435	45	11.5	0.5	21	231
14	16.5	0.5	29	435	46	11.5	0.5	21	231
15	16.5	0.5	29	435	47	11.5	0.5	21	231
16	16.5	0.5	29	435	48	11.5	0.5	21	231
17	15	0.5	28	406	49	11.5	0.5	21	231
18	15	0.5	28	406	50	7.5	0.5	13	91
19	15	0.5	28	406	51	7.5	0.5	13	91
20	15	0.5	28	406	52	7.5	0.5	13	91
21	7.5	0.5	13	91	53	7.5	0.5	13	91
22	7.5	0.5	13	91	54	7.5	0.5	13	91
23	7.5	0.5	13	91	55	7.5	0.5	13	91
24	7.5	0.5	13	91	56	7.5	0.5	13	91
25	7.5	0.5	13	91	57	7.5	0.5	13	91
26	15	0.5	28	406	58	7.5	0.5	13	91
27	15	0.5	28	406	59	7.5	0.5	13	91
28	15	0.5	28	406	60	7.5	0.5	13	91
29	15	0.5	28	406	61	7.5	0.5	13	91
30	15	0.5	28	406	62	7.5	0.5	13	91
31	14.5	0.5	27	378					
32	14.5	0.5	27	378					

voltage at the receiving dipole. The MAE instrument allows automatic averaging of up to 10 measures of the input voltage. In bad noise conditions, the stacking cycle can, of course, be iterated as many times as needed until reaching a stable average value. The third way is to increase one or both dipole lengths, which has also the advantage of increasing the sensitivity of the array with depth (Edwards 1977). Using this last approach, in order to realize the same grid of datum points as in Figure 2, care must be taken not to change the positions of the centres of the dipoles. Using all of the three approaches, we have been able to fulfil the entire acquisition plan listed in Table 1.

In order to accommodate the wide resistivity range detected inside the Bedestan and to better show order of magnitude changes, a common logarithmic scale has been used for visualization of both apparent resistivity and modelled real resistivity maps (for the use of logarithmic scales in geoelectrics, see, e.g., Chambers *et al.* 2006).

Figure 4 *The multi-electrode device spread out on the floor of the Bedestan interior.*

Figure 5 shows a sequence of horizontal slices, depicting the contoured apparent resistivity values at increasing pseudodepths. A variation of the apparent resistivity from 10 ohm·m to about 400 ohm·m can readily be observed, with a concentration of apparent resistivity highs below the front half of the Bedestan complex, which are well distinguished from an area of almost uniform low apparent resistivity values in the rear half of the complex. Since stone ruins should be, at least in principle, more resistive than the alluvial soil that characterizes the surface geology in the area (Atalar 2011), the remains of the earlier Byzantine basilica were supposed to have some chance of being found only beneath the front half of the Bedestan. To better investigate such a possibility, data modelling has been undertaken using the PERTI algorithm, whose methodological steps are briefly recalled in the following section.

OUTLINE OF THE PERTI METHOD

The PERTI method is a straight derivation of the probability tomography imaging approach, which consists of mapping the spatial behaviour of the resistivity anomaly occurrence probability index $\eta(\mathrm{P}_q)$, calculated at a grid of points P_q ($q = 1, 2, \ldots, Q$) below the ground surface by Mauriello and Patella (1999):

$$\eta(\mathrm{P}_q) = C_q \sum_{m=1}^{M} \sum_{j_m=1}^{J_m} [\rho_a(\mathrm{P}_{j_m}) - \hat{\rho}] \Psi(\mathrm{P}_{j_m}, \mathrm{P}_q). \quad (1)$$

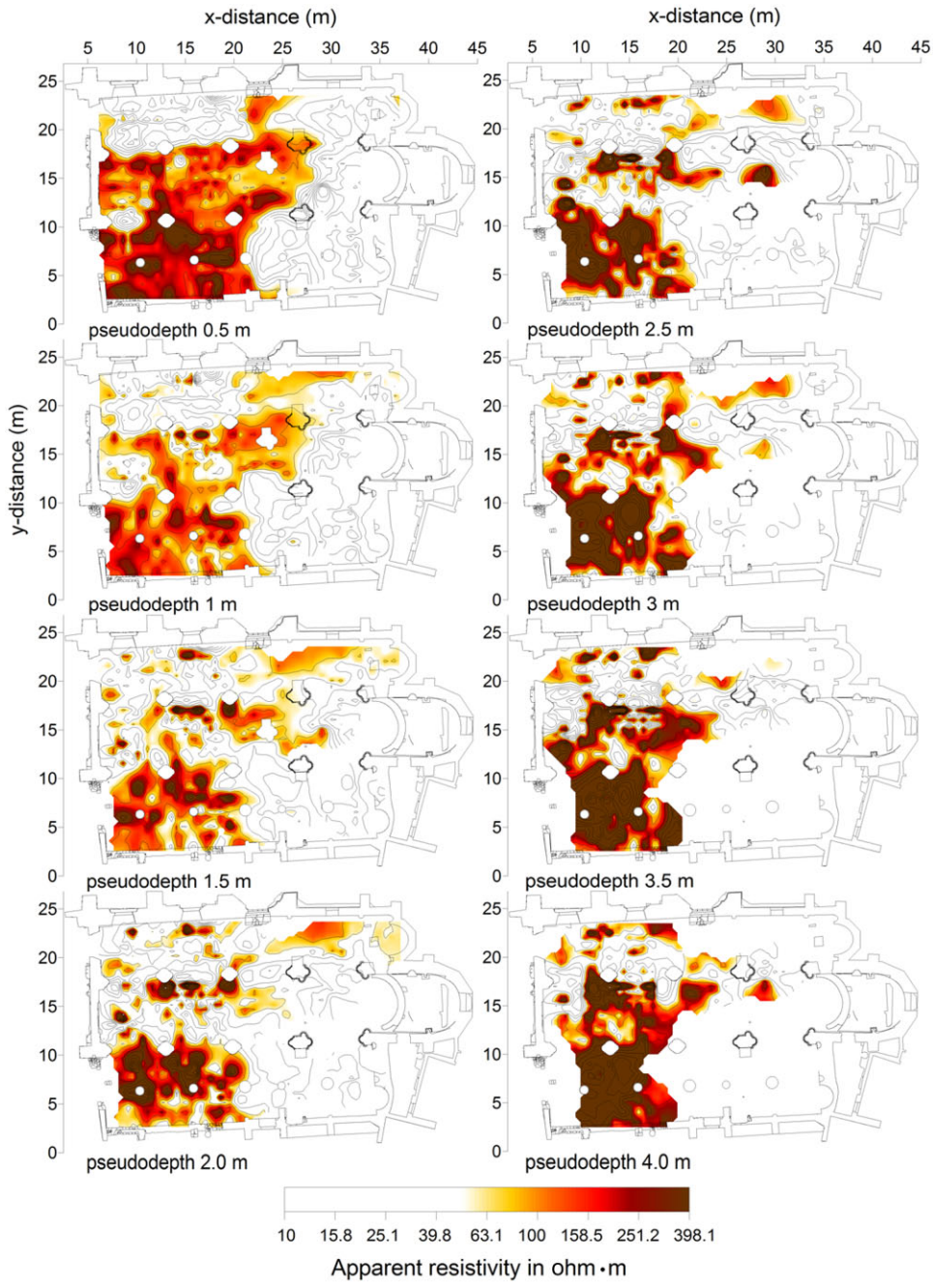

Figure 5 *Contoured apparent resistivity maps on horizontal slices at different pseudodepths, drawn by considering all of the longitudinal and transversal ERT profiles reported in Figure 3.*

In equation (1), $\rho_a(\mathrm{P}_{j_m})$ is the measured apparent resistivity at P_{j_m}; that is, the j_mth nodal attribution point of the mth profile ($j_m = 1, \ldots, J_m$; $m = 1, \ldots, M$), corresponding to $\rho_a(l, n)$ in Figure 2; $\hat{\rho}$ is a pre-assigned resistivity of a homogeneous, isotropic half-space assumed as reference model; C_q is a positive-definite non-null normalization factor; $\Psi(\mathrm{P}_{j_m}, \mathrm{P}_q)$, often called the sensitivity function of the array, is the j_mth Frechet derivative referred to the reference model. It physically describes the effect generated at P_{j_m} by a small perturbation of the reference resistivity at P_q, under Born approximation (Loke and Barker 1995, 1996; Mauriello and Patella 1999).

In practice, the average apparent resistivity is assumed as the reference uniform resistivity $\hat{\rho}$. Therefore, $\eta(\mathrm{P}_q)$ is interpreted as an occurrence probability measure of a resistivity deviation from $\hat{\rho}$ at P_q. Positive or negative values of $\eta(\mathrm{P}_q)$ give the occurrence probability of an increase or decrease of resistivity, respectively.

Many field cases were dealt with using this approach (e.g., Cammarano *et al*. 2000; Di Fiore *et al*. 2002; Alaia *et al*. 2008; Compare *et al*. 2009a,b). In all cases, the 2D or 3D probability tomography mapping of the $\eta(\mathrm{P}_q)$ function given by equation (1) proved to be a reliable tool for recognizing the most probable location of the buried anomaly source centres, compatible with the available data set.

Using equation (1), no information can, however, be deduced with regard to estimation of the real resistivity distribution. The PERTI method has been formulated just to find a solution to this last problem in the framework of the probability tomography.

The starting assumption for the PERTI method is that the reference resistivity $\hat{\rho}$ must not be pre-assigned, but assumed to be the unknown true resistivity value ρ_q at P_q. With such an assumption, $\eta(\mathrm{P}_q)$ given in equation (1) can be rewritten as

$$\eta(\mathrm{P}_q) = C_q \sum_{m=1}^{M} \sum_{j_m=1}^{J_m} [\rho_a(\mathrm{P}_{j_m}) - \rho_q]\, \Psi(\mathrm{P}_{j_m}, \mathrm{P}_q). \tag{2}$$

The rationale for the PERTI approach is that if $\eta(\mathrm{P}_q) = 0$ occurs at P_q, then the most probable real resistivity there would be exactly ρ_q. Thus, referring to equation (2), since it is always $C_q \neq 0$, the $\eta(\mathrm{P}_q) = 0$ condition allows the following inversion formula to be easily derived (Mauriello and Patella 2009):

$$\rho_q = \frac{\displaystyle\sum_{m=1}^{M} \sum_{j_m=1}^{J_m} \rho_a(\mathrm{P}_{j_m})\, \Psi(\mathrm{P}_{j_m}, \mathrm{P}_q)}{\displaystyle\sum_{m=1}^{M} \sum_{j_m=1}^{J_m} \Psi(\mathrm{P}_{j_m}, \mathrm{P}_q)}. \tag{3}$$

The most probable real resistivity ρ_q at P_q, compatible with data accuracy and density and within the assumed first-order Born approximation, is simply derived as the weighted average of the apparent resistivity values, using as weights the sensitivity function of the array. Thus, the PERTI formula (3) can easily be converted into a user-friendly algorithm, quite apt to combine a great multiplicity of large data sets.

The main features of the PERTI method, amply discussed in Mauriello and Patella (2009), are: (i) independence from *a priori* information; (ii) the absence of iterative processes; (iii) the drastic reduction of computing time, of two orders of magnitude, at least, with respect to standard deterministic inversion tools; (iv) independence from data acquisition

techniques and spatial regularity; (v) the capability to resolve complex continuous resistivity variation.

Besides these advantages, the synthetic examples discussed in Mauriello and Patella (2009) have also shown, however, a reduced ability of the PERTI algorithm to provide resistivity values close to reality in the case of large resistivity contrasts. Furthermore, the PERTI algorithm can project shallow bodies to deeper levels, mainly when dipoles larger than their depth of burial are used. However, it must be noted that such deeper projections can also be considered an equivalent solution, fully compatible with the available data set. A similar effect was also observed and amply discussed in gravity probability tomography (Mauriello and Patella 2001, esp. p. 1435, fig. 3). Finally, remembering that the PERTI method uses the sensitivity values as weighting factors, the reconstructed images at the shallower layers will inevitably be affected by the higher amplitudes of the sensistivity at very shallow depths, so that the risk of near-surface artefacts cannot be excluded.

In conclusion, PERTI is, in principle, a probability-based sensistivity inversion method, whose reconstructed images can be used for an approximate estimate of the anomalies in the field. It is worth implementing the PERTI methodology where fast inversion is required, in some cases sacrificing the resolution or accuracy, which can be reached by standard deterministic inversion tools at the expense of much greater computation time and more resources.

A direct consequence of not requiring *a priori* information and iterative processes is, for the PERTI method, the uselessness of the computation of the RMS error between the measured and modelled apparent resistivity values. In fact, the resulting RMS error, whatever it is, could not be lowered in any way, within the PERTI theory. The only way to judge the modelling quality of the PERTI method is by comparison with other standardized deterministic inversion tools.

THE PERTI RESULTS AT THE BEDESTAN

Figure 6 shows a sequence of horizontal slices reporting the modelled real resistivity maps at increasing depths below ground level, obtained using the PERTI formula (3) and including all of the profiles located as in Figure 3. The computation time required by the PERTI algorithm to provide the entire resistivity model on a standard PC has been of the order of only some tens of seconds.

A three-room rectangular space, delimited all around and inside by sets of aligned resistive blocks with resistivity in the range 100–400 ohm·m, appears in all of the slices from 0.25 m to 2.0 m depth, at most, in the ranges 6–21 m and 3–23 m along the *x*- and *y*-axes, respectively. Moreover, in all of the slices from 0.25 m to 1.0 m depth, a resistive rounded structure with a mean resistivity of about 150 ohm·m appears in the ranges 20–25 m and 12–18 m along the *x*- and *y*-axes, respectively. Altogether, these resistive features, showing in plan the shape of a church characterized by a central nave with an apse and two side aisles, have been interpreted as evidence of the existence of remains of the earlier Byzantine basilica. In particular, out of the sets of aligned resistive blocks, the two inner ones have been assumed to represent remains of columns and/or arches dividing the basilica's central nave from its two side aisles and the outer ones the remains of the peripheral walls. Furthermore, the rounded structure has been assumed to represent the remains of the back wall of the apse of the basilica. All of these resistive features appear immersed in a conductive layer with resistivity in the range 20–40 ohm·m, very likely ascribable to fills originated by the recurrent streams of alluvial soil that, right up to the present time, seasonally continue to invade the whole territory of Nicosia (Atalar 2011). To better focus the footprint of the churchlike structure, Figure 7 (a) shows the same PERTI slice of Figure 6 at

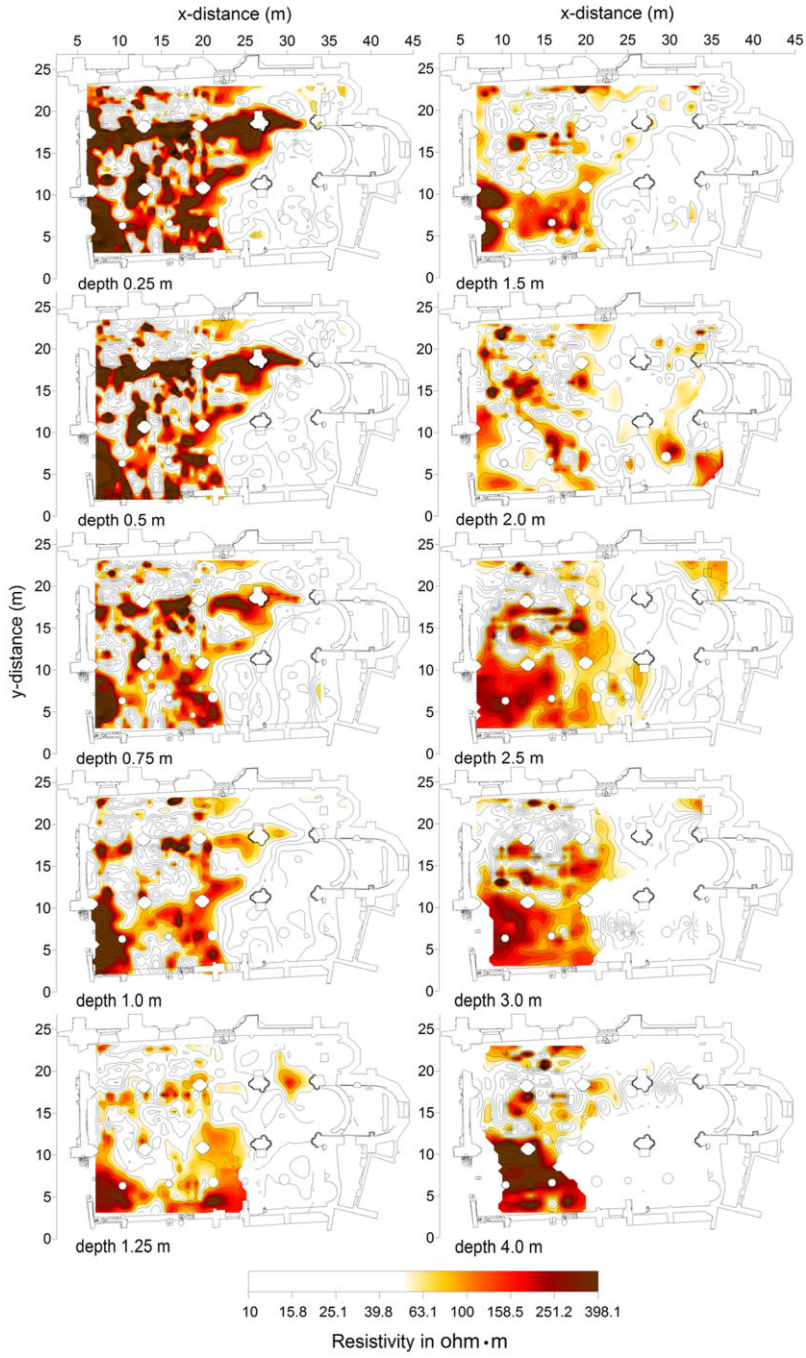

Figure 6 *Modelled real resistivity maps at increasing depths below ground level, constructed by the PERTI method considering all of the ERT profiles reported in Figure 3.*

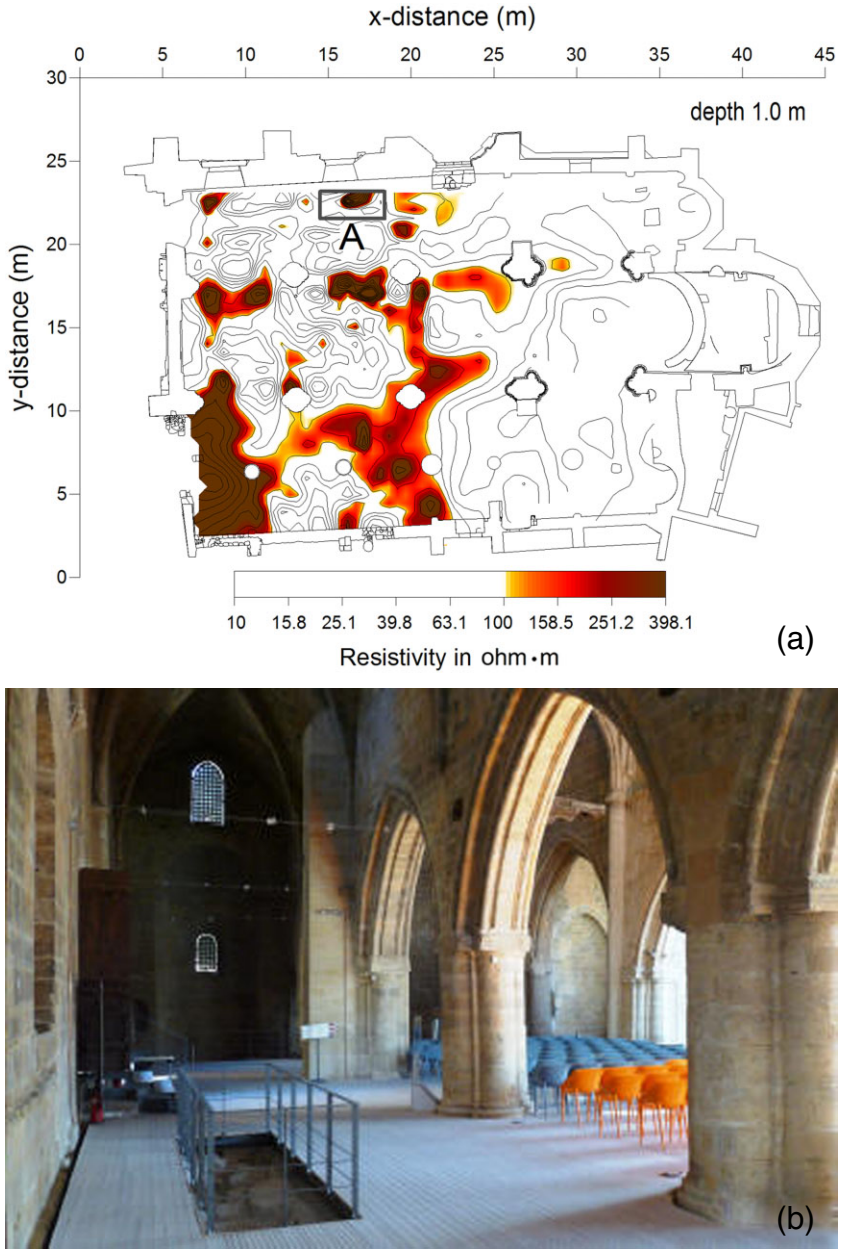

Figure 7 *(a) The modelled resistivity map at 1 m depth, extracted from Figure 6 to highlight the presence of the high-resistivity churchlike structure. The rectangle marked 'A' indicates the area where excavations have been carried out. (b) The Bedestan complex after restoration, with exposure of foundations of the Byzantine church's peripheral wall, discovered in the rectangular area marked 'A' in (a) (from www.whatson-northcyprus.com).*

1 m depth, where only the scale range 100–398.1 ohm·m is highlighted. Excavations down to a depth of about 0.5 m in the area marked 'A' in Figure 7 (a) have, as predicted, brought to light the existence of blocks of masonry (Fig. 7 (b)).

At last, worth mentioning are also some small volumes, randomly distributed under the surveyed area, showing resistivity values in the range 10–12.6 ohm·m. To better focus their presence, Figure 8 (a) shows the same PERTI slice of Figure 6 at 0.5 m depth, where only the scale range 10–12.6 ohm·m is highlighted. Excavations down to that depth in the area marked 'B' in Figure 8 (a) have brought to light the existence of tombs filled with wet clayey soil and debris (Fig. 8 (b)).

In order to combine the PERTI results in a unique 3D representation and give some more insight into the observed anomalies, Figure 9 shows images of the resistivity model space under two opposite angles of view. To better highlight the nature and shape of the resistive structures, four increasingly smaller subspaces have been contoured, using, progressively, 63.1, 100, 158.5 and 251.2 ohm·m as the cut-off resistivity. All of the contoured surfaces corresponding to resistivity values below the cut-off resistivity have been blanked.

Looking at Figure 9, two important considerations can be made. The first concerns the possibility of evaluating, qualitatively, the degree of degradation of the remains attributed to the Byzantine basilica: the lower the resistivity of the stone blocks, the higher is the level of degradation, probably due to infiltration of water into the vadose zone, where the remains lie. In this respect, the level of degradation appears to increase, passing from the right aisle to the left aisle, in which a nearly uniform basin, filled with conductive wet ground, appears in continuity with the nature of the subsoil under the rear half of the Bedestan complex.

The second consideration concerns the presence of a shapeless volume of high-resistivity material at the front portion of the right aisle of the earlier basilica, which was already evident in Figure 6 in all of the horizontal slices from 2.5 m to 4.0 m depth. A possible interpretation is to associate this amorphous volume with debris of stone blocks collapsed inside the church or deposited from outside.

COMPARISON BETWEEN PERTI AND ERTLAB MODELLING RESULTS

As previously said, this contribution provides one of the first applications of the PERTI tool to large field data sets. To fully appreciate its modelling capability and reliability, we now discuss the comparison with the results depicted in Figure 10, obtained by the ERTLab inversion software. A heavy limitation of this software has been the extremely long computation time, of the order of tens of hours, required to elaborate the whole field data set with the same PC used for the PERTI elaboration. Furthermore, the ERTLab software has not allowed the mapping of slices deeper than 2.5 m. No instruction is given in the ERTLab user's manual on how to tackle such an apparent shortcoming, so we are unable to decide whether it is a deficiency of the solver module or of the graphical viewer, or of both environments.

Therefore, limiting the analysis to the depth range from 0.25 m to 2.5 m, the comparison between PERTI and ERTLab shows a general agreement, as regards the features of the main resistive structures. Nevertheless, two significant differences can be observed. The first concerns the shallower layers, where the ERT measurements exhibit the highest sensitivity values, and the probability of the inversion algorithm generating artefacts is higher. In this respect, in the depth range from 0.25 m to 1.50 m, where the traces of the churchlike structure are outlined, the PERTI model appears less affected than the ERTLab solution. The second difference refers to the deeper levels, where the ERT measurements have, instead, the lowest sensitivity values. In the two

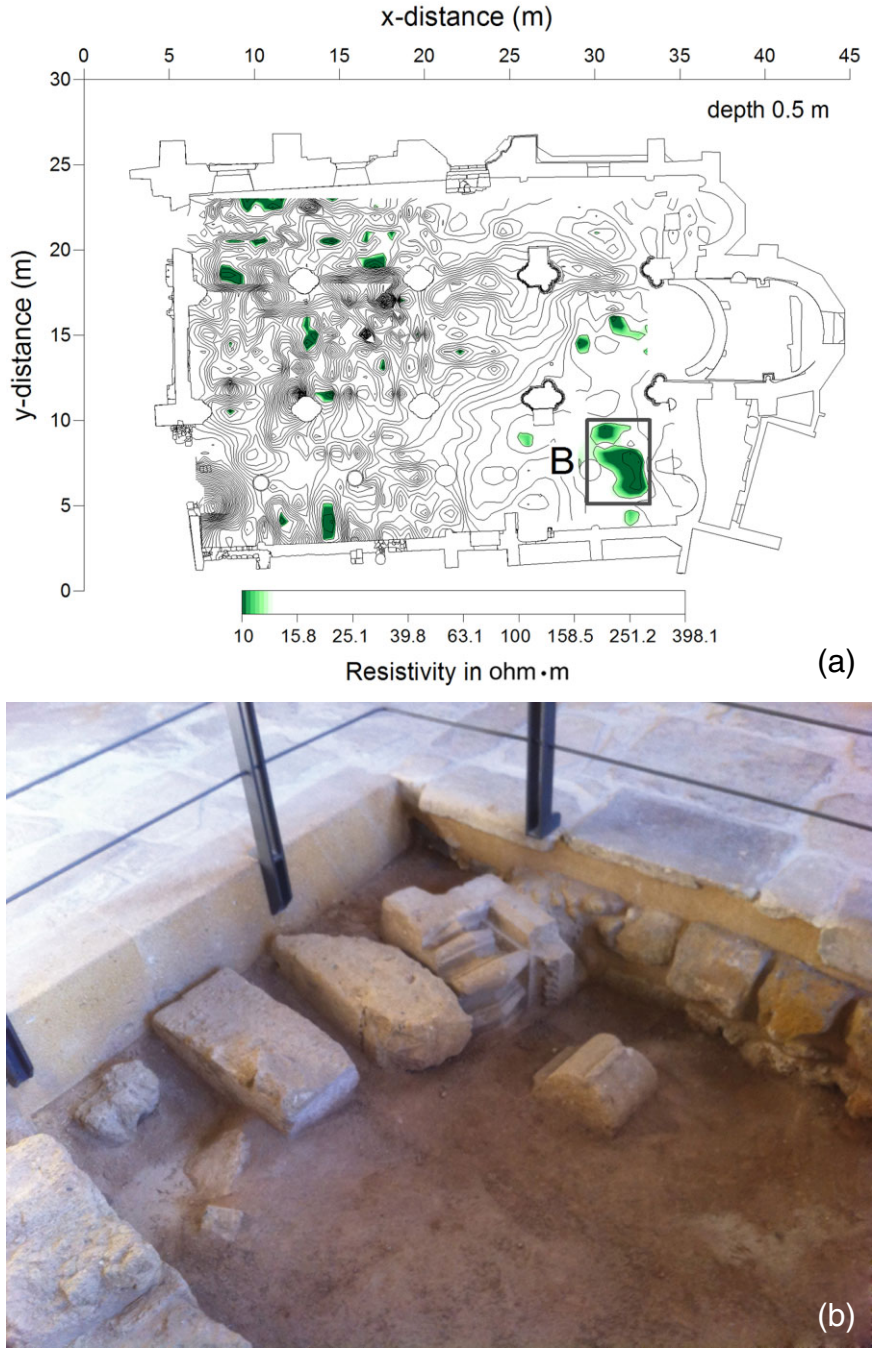

Figure 8 *(a) The modelled resistivity map at 0.5 m depth, extracted from Figure 6 to highlight the presence of randomly distributed high-conductivity volumes. The rectangle marked 'B' indicates the area where excavations have been carried out. (b) The Bedestan complex after restoration, with exposure of foundations of the burial site, discovered in the rectangular area marked 'B' in (a).*

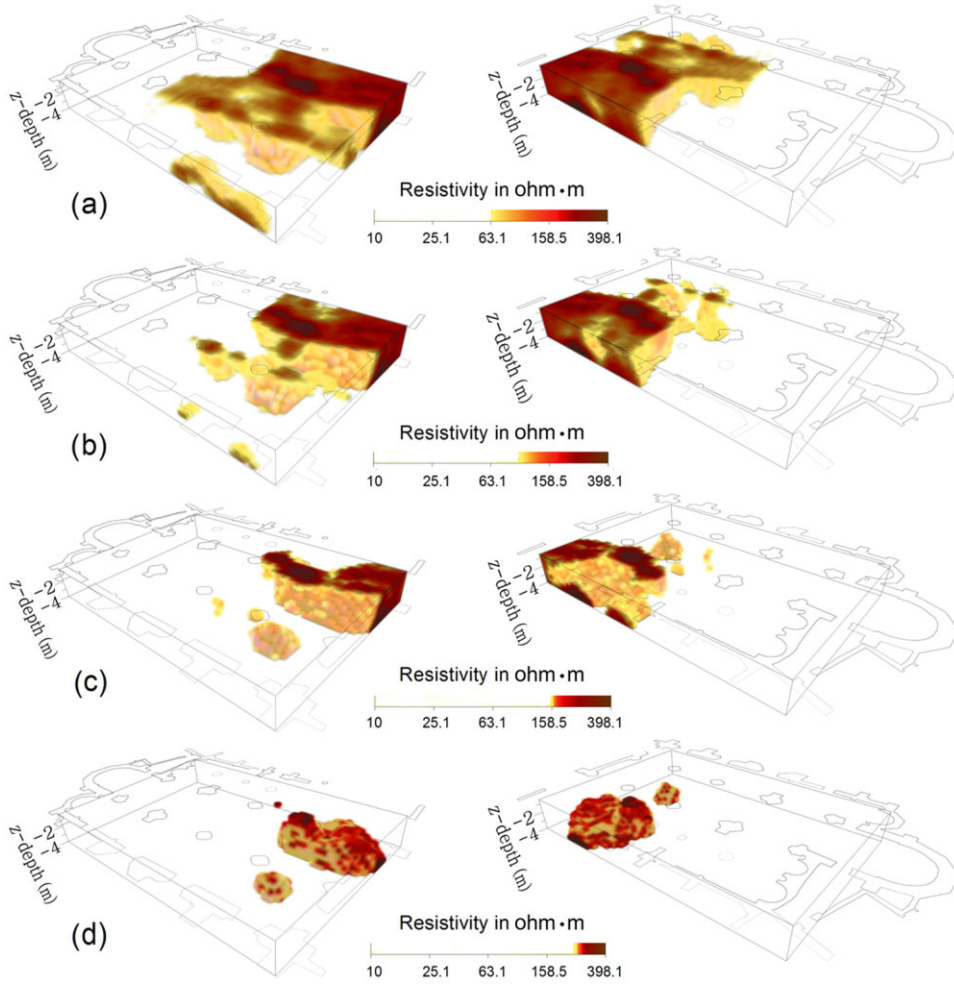

Figure 9 *3D imaging of the PERTI results under two opposite angles of view. The four different pairs from top to bottom correspond to an increasing high-pass cut-off resistivity, namely (a) 63.1, (b) 100, (c) 158.5 and (d) 251.2 ohm·m.*

deepest ERTLab maps, the high-resistivity signature tends to expand over the entire central-right portion of the front half of the Bedestan, while in the PERTI maps at the same depths the same structure appears concentrated in a more restricted space.

A synthetic way to visualize the degree of similitude between the PERTI and ERTLab models is to map a dimensionless discrepancy index. We define this index as the per cent ratio of the difference between the PERTI and ERTLab resistivity values to the ERTLab resistivity, calculated point by point. An example of such a computation is the map reported in Figure 11, using the PERTI and ERTLab slices at 0.5 m depth, extracted from Figures 6 and 10, respectively. For this ERTLab map, the RMS deviation between the observed and modelled apparent resistivity values turned out to be 8.6 ohm·m.

An overall similarity can be observed between the map in Figure 11 and the parent maps of Figures 6 and 10, mostly that of Figure 6. In fact, the highest positive values of the discrepancy

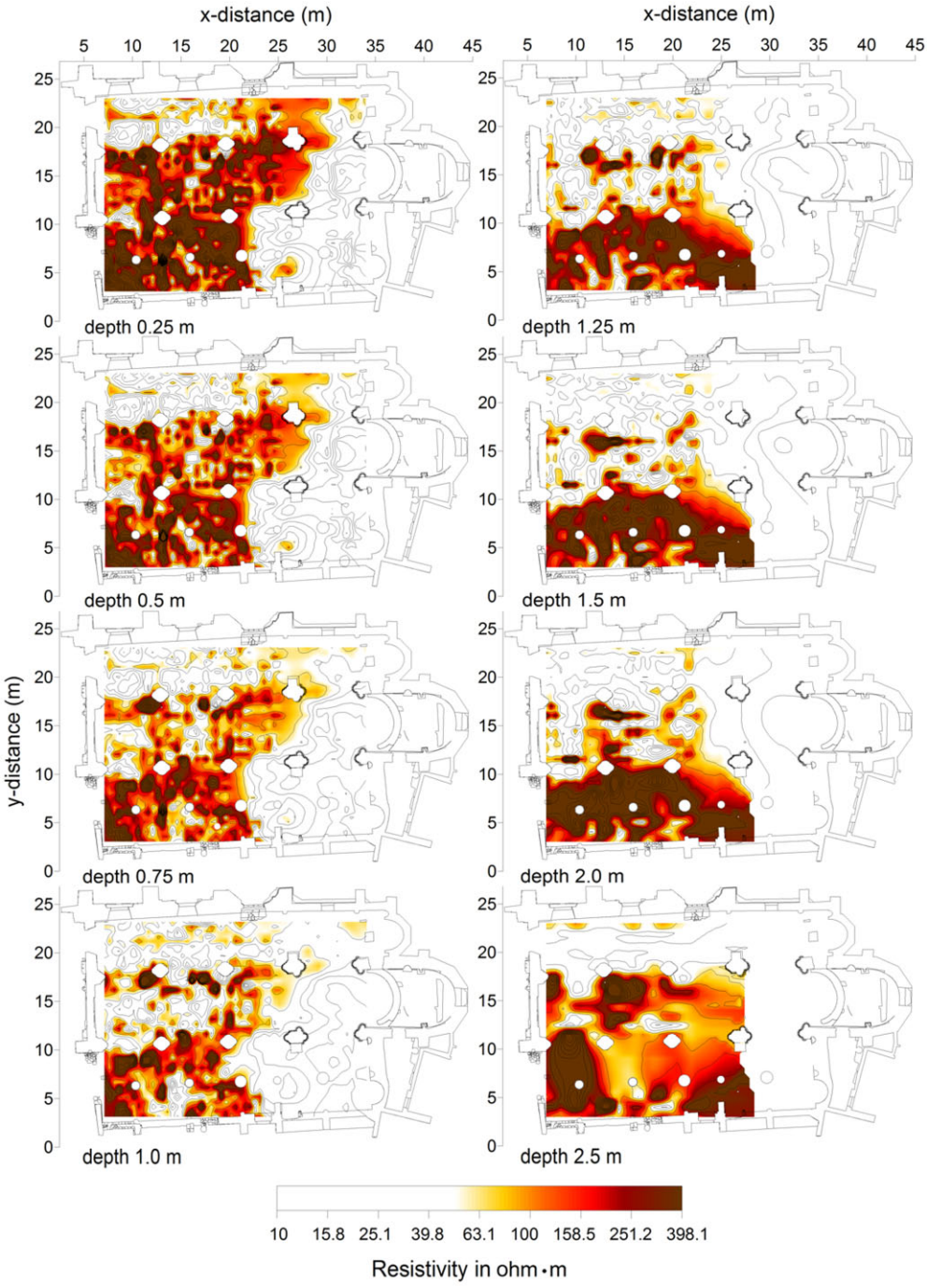

Figure 10 *Modelled real resistivity maps at increasing depths below ground level, constructed by the ERTLab method considering all of the ERT profiles reported in Figure 3.*

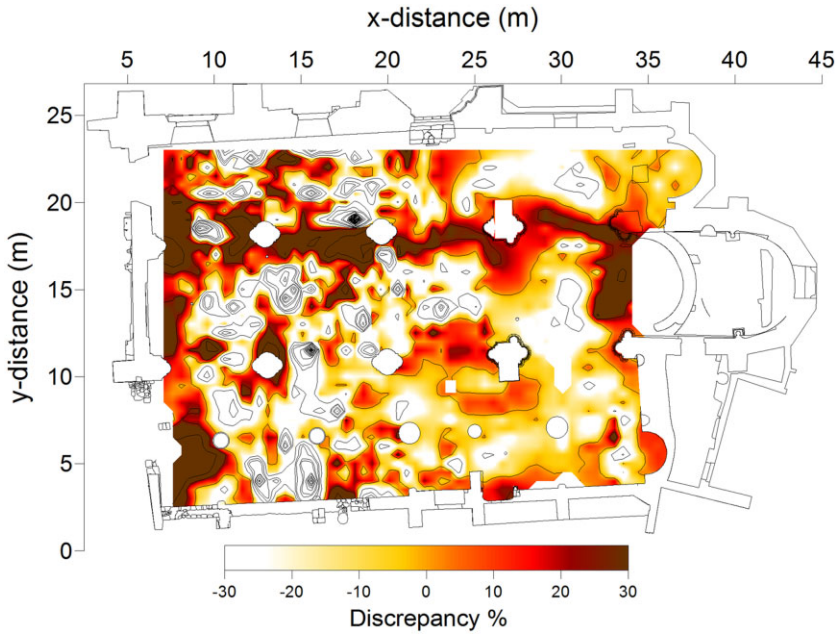

Figure 11 *A map showing the behaviour of the dimensionless discrepancy index, defined as the per cent ratio of the difference between the PERTI and ERTLab resistivity values, to the ERTLab resistivity, relative to the PERTI and ERTLab modelled resistivity maps at 0.5 m depth, extracted from Figures 6 and 10, respectively.*

index tend to aggregate in such a way as to resemble the sets of resistive blocks, while the lowest negative values mainly fall in the areas where the structures with lowest resistivity have been found. Therefore, in this example, the PERTI algorithm seems to generate a model with a resistivity contrast between the least and the most resistive structures that is slightly higher than that generated by the ERTLab inversion. The RMS discrepancy between the PERTI and ERTLab model resistivity values in the map of Figure 11 is 0.7335 ohm·m.

CONCLUSIONS

In the framework of a project for the rehabilitation of Old Nicosia, Cyprus, a geoelectrical survey has been planned inside the Bedestan monumental complex, aimed at detecting and localizing remains of a pre-existing Byzantine basilica beneath the floor of the complex.

The geoelectrical survey was carried out using a dipole–dipole electrode array, moved along a multiple set of profiles distributed almost regularly on the floor of the complex. The probability-based electrical resistivity tomography inversion (PERTI) tool has been applied to interpret the detected geoelectrical anomalies, mainly because it does not require any external *a priori* information, it is computationally simple and fast, and it is independent from irregularities in data spatial distribution.

The main features highlighted in the first 4 m depth range below the ground are: (i) aligned sets of resistive blocks with resistivity in the range 100–400 ohm·m, the inner ones of which have been ascribed to relics of columns and/or arches dividing the older church's nave from its two

side aisles, and the outer ones to relics of the peripheral walls; and (ii) a rounded resistive structure with an average resistivity of about 150 ohm·m, which has been ascribed to relics of the rear wall of an apsis. All of these highly resistive features appear immersed in a conductive cover with resistivity around 20–40 ohm·m, composed of alluvial soil probably deposited over the whole area from the sixth to the 12th century.

Taking into account the ERT results, the consolidation and conservative restoration programme of the Bedestan complex was redesigned by including the installation of wood flooring, floating above the original stone floor, in order to preserve the detected buried archaeological heritage (Cessari and Gigliarelli 2007). Ground-truth was, therefore, limited to just two sites. The first site was one where a high-resistivity anomaly source was found stretching along the border to the left of the left aisle of St Nicholas, which was ascertained to be remains of masonry, probably attributable to a side wall of the earlier Byzantine basilica. The second site was one in which a volume with high conductivity was detected as the source of the anomaly in the right sector of the rear part of the Bedestan, which was found to contain remains of graves.

In conclusion, with regard to this first application of PERTI to a real field data set, we feel we can say that the method has shown a very promising potential in archaeological prospecting, where it may be used as a fast deconvolution filter, providing information regarding the size, shape and depth of burial of the archaeological structures and a reasonable estimation of their resistivity.

After a 5-year recovery action, in November 2009 the Bedestan complex was finally reopened as a multicultural venue and exhibition space (InMotion 2012).

ACKNOWLEDGEMENTS

This study was performed in the framework of the ‘Rehabilitation of Old Nicosia’ EU–UNDP project. The authors wish to thank the two anonymous referees for their constructive criticisms.

REFERENCES

Abu Zeid, N., Balducci, M., Bartocci, F., Regni, R., and Santarato, G., 2009, Indirect estimation of injected mortar volume in historical walls using the electrical resistivity tomography, *Journal of Cultural Heritage*, **11**, 220–7.

Alaia, R., Patella, D., and Mauriello, P., 2008, Application of the geoelectrical 3D probability tomography in a test-site of the archaeological park of Pompei (Naples, Italy), *Journal of Geophysics and Engineering*, **5**, 67–76.

Atalar, C., 2011, A review of the origin and properties of the soils of Nicosia, Cyprus, *International Journal of Geotechnical Engineering*, **5**, 79–86.

Bavusi, M., Giocoli, A., Rizzo, E., and Lapenna, V., 2009, Geophysical characterisation of Carlo’s V Castle (Crotone, Italy), *Journal of Applied Geophysics*, **67**, 386–401.

Boase, T. S. R., 1977, The arts in Cyprus. A. Ecclesiastical art, in *A history of the Crusades, vol.4: the art and architecture of the Crusader States* (ed. H. W. Hazard), The University of Wisconsin Press, Madison, WI.

Cammarano, F., Di Fiore, B., Patella, D., and Mauriello, P., 2000, Examples of application of electrical tomographies and radar profiling to cultural heritage, *Annals of Geophysics*, **43**, 309–24.

Cammarano, F., Mauriello, P., Patella, D., and Piro, S., 1997, Geophysical methods for archaeological prospecting: a review, *Science and Technology for Cultural Heritage*, **6**, 151–73.

Candansayar, M. E., Basokur, A. T., and Peksen, E., 1999, Detecting small-scale targets by the two-sided gradient transformation, *Journal of the Balkan Geophysical Society*, **2**, 100–11.

Cardarelli, E., Fischanger, F., and Piro, S., 2008, Integrated geophysical survey to detect buried structures for archaeological prospecting: a case-history at Sabine Necropolis (Rome, Italy), *Near Surface Geophysics*, **6**, 15–20.

Cessari, L., and Gigliarelli, E., 2007, From architectural diagnostics to conservation strategies: the case for the Bedestan (Cyprus), *Actes du Rencontre Internationale sur le Patrimoine Architectural Méditerranéen*, 1–14, Université Moulay Ismail, Faculté des Sciences, Meknes, Maroc.

Chambers, J. E., Kuras, O., Meldrum, P. I., Ogilvy, R. D., and Hollands, J., 2006, Case history—electrical resistivity tomography applied to geologic, hydrogeologic, and engineering investigations at a former waste-disposal site, *Geophysics*, **71**, B231–9.

Compare, V., Cozzolino, M., Mauriello, P., and Patella, D., 2009a, Resistivity probability tomography at the Castle of Zena (Italy), *EURASIP Journal on Image and Video Processing*, vol. 2009, Article ID 693274, 9 pp.

Compare, V., Cozzolino, M., Mauriello, P., and Patella, D., 2009b, Three-dimensional resistivity probability tomography at the prehistoric site of Grotta Reali (Molise, Italy), *Archaeological Prospection*, **16**, 53–63.

Di Fiore, B., Mauriello, P., Monna, D., and Patella, D., 2002, Examples of application of the tensorial resistivity probability tomography to architectonic and archaeological targets, *Annals of Geophysics*, **45**, 417–29.

Drahor, M. G., Berge, M. A., Kurtulmuş, T. Ö., Hartmann, M., and Speidel, M. A., 2008a, Magnetic and electrical resistivity tomography investigations in a Roman legionary camp site (*Legio IV Scythica*) in Zeugma, SE Anatolia, Turkey, *Archaeological Prospection*, **15**, 159–86.

Drahor, M. G., Kurtulmuş, T. Ö., Berge, M. A., Hartmann, M., and Speidel, M. A., 2008b, Magnetic imaging and electrical resistivity tomography studies in a Roman military installation found in Satala archaeological site, northeastern Anatolia, Turkey, *Journal of Archaeological Science*, **35**, 259–71.

Edwards, L. S., 1977, A modified pseudosection for resistivity and induced-polarization, *Geophysics*, **42**, 1020–36.

Gaffney, C., 2008, Detecting trends in the prediction of the buried past: a review of geophysical techniques in archaeology, *Archaeometry*, **50**, 313–36.

Hecht, S., 2009, Viewing the subsurface in 3D: sediment tomography for (geo-) archaeological prospection in Palpa, southern Peru, in *Natural science in archaeology: new technologies for archaeology* (eds. M. Reindel and G. A. Wagner), Part II, 87–102, Springer-Verlag, Berlin.

InMotion Productions, 2012, *The Bedestan—a cultural journey across ages*, Video production for UNDP, Nicosia, Cyprus, www.InMotion.video

Jeffery, G., 1918, *A description of the historic monuments of Cyprus: studies in the archaeology and architecture of the island*, W. J. Archer, G.P.O., Nicosia, Cyprus.

Kampke, A., 1999, Focused imaging of electrical resistivity data in archaeological prospecting, *Journal of Applied Geophysics*, **41**, 215–27.

Loke, M. H., 2012, *Tutorial: 2-D and 3-D electrical imaging surveys*, 1–161, Geotomo Softwares, Penang, Malaysia. www.geotomosoft.com

Loke, M. H., and Barker, R. D., 1995, Least-squares deconvolution of apparent resistivity pseudosections, *Geophysics*, **60**, 1682–90.

Loke, M. H., and Barker, R. D., 1996, Rapid least-squares inversion of apparent resistivity pseudosections by a quasi-Newton method, *Geophysical Prospecting*, **44**, 131–52.

Matias, H. C., Monteiro Santos, F. A., Rodrigues Ferreira, F. E., Machado, C., and Luzio, R., 2006, Detection of graves using the micro-resistivity method, *Annals of Geophysics*, **49**, 1235–44.

Mauriello, P., and Patella, D., 1999, Resistivity anomaly imaging by probability tomography, *Geophysical Prospecting*, **47**, 411–29.

Mauriello, P., and Patella, D., 2001, Localization of maximum-depth gravity anomaly sources by a distribution of equivalent point masses, *Geophysics*, **66**, 1431–7.

Mauriello, P., and Patella, D., 2009, A data-adaptive probability-based fast ERT inversion method, *Progress in Electromagnetics Research*, **97**, 275–90.

Mauriello, P., Monna, D., and Patella, D., 1998, 3D geoelectric tomography and archaeological applications, *Geophysical Prospecting*, **46**, 543–70.

Mol, L., and Preston, P. R., 2010, The writing's in the wall: a review of new preliminary applications of electrical resistivity tomography within archaeology, *Archaeometry*, **52**, 1079–95.

Noel, M., and Xu, B., 1991, Archaeological investigation by electrical resistivity tomography: a preliminary study, *Geophysical Journal International*, **107**, 95–102.

Nuzzo, L., Leucci, G., and Negri, S., 2009, GPR, ERT and magnetic investigations inside the Martyrium of St Philip, Hierapolis, Turkey, *Archaeological Prospection*, **16**, 177–92.

Papadopoulos, N., Sarris, A., Yi, M. J., and Kim, J. H., 2008, Urban archaeological investigations using surface 3D ground penetrating radar and electrical resistivity tomography methods, *Exploration Geophysics*, **40**, 56–68.

Qantara, 2008, *The Greek cathedral in Nicosia: Bedestan*, Mediterranean Heritage, Euromed Heritage programme, www.qantara-med.org

Ranieri, G., Sharpe, L., Trogu, A., and Piga, C., 2007, Time-lapse electrical resistivity tomography to delineate mud structures in archaeological prospections, *Near Surface Geophysics*, **5**, 375–82.

Tsokas, N. G., and Tsourlos, P. I., 1997, Transformation of the resistivity anomalies from archaeological sites by inversion filtering, *Geophysics*, **62**, 36–43.

Tsokas, N. G., Tsourlos, P. I., Stampolidis, A., Katsonopoulou, D., and Soter, S., 2009, Tracing a major Roman road in the area of ancient Helike by resistivity tomography, *Archaeological Prospection*, **16**, 251–66.

Ward, S. H., 1990, Resistivity and induced polarization methods, in *Geotechnical and environmental geophysics, vol. I: review and tutorials* (ed. S. H. Ward), 147–89, Investigations in Geophysics No. 5, Society of Exploration Geophysicists, Tulsa, OK.